A Dynamic Density Functional Study of the Stepwise Migratory Insertion of Isocyanides into Zirconium−Carbon Bonds Anchored to a Calix[4]arene Moiety

Simona Fantacci,* Filippo De Angelis, and Antonio Sgamellotti

Istituto CNR di Scienze e Tecnologie Molecolari (ISTM) c/o Dipartimento di Chimica, Università di Perugia, I-06123 Perugia, Italy

Nazzareno Re

Facoltà di Farmacia, Università G. D'Annunzio, I-66100 Chieti, Italy

Received April 1, 2002

The stepwise migratory insertion of methyl isocyanide into the zirconium−carbon bonds in [calix[4](OMe)$_2$(O)$_2$-ZrMe$_2$] has been investigated by means of both static and dynamic density functional calculations. Dynamics simulations have shown that methyl isocyanide insertion takes place via the initial formation of an η^1-iminoacyl species that is suddenly converted into the more stable η^2-isomer. The energy profiles for the two pathways branching from the initially formed η^2-iminoacyl, i.e., (i) the insertion of a second isocyanide molecule into the residual alkyl group leading to a bis-η^2-iminoacyl and (ii) the insertion of the residual alkyl group into the iminoacyl moiety leading to an η^2-bound imine, have been characterized. Formation of the bis-η^2-iminoacyl species was found to be thermodynamically favored at low temperature ($\Delta G^{\ddagger}$ =7.2 vs 6.4 kcal mol^{-1}, ΔE = −38.5 vs −12.2 kcal mol^{-1}). However, the large entropic contribution to the barrier for this intermolecular process kinetically favors the intramolecular imine formation at room temperature ($\Delta G^{\ddagger}$ =11.5 vs 6.4 kcal mol^{-1}), providing a rationale for the experimentally characterized temperature selectivity of the overall reaction.

Downloaded by CARLI CONSORTIUM on June 29, 2009
Published on August 28, 2002 on http://pubs.acs.org | doi: 10.1021/om020250j

Introduction

Migratory insertion of carbon monoxide or isocyanides into M−X bonds (X = alkyl, hydrido, silyl, amido, phosphido) is one of the most exciting fields of research in organometallic chemistry because of the reactivity of the resulting products and their involvement in many stoichiometric and catalytic applications.[1−3] The migratory insertion of carbon monoxide in metal−alkyl bonds has been observed for most of the early d-block metals, as well as numerous actinide and lanthanide elements, and has received much attention from synthetic, mechanistic, and theoretical points of view.[1−8] Spectroscopic data and structural studies have indicated that all isolable CO insertion products contain η^2-acyl groups, where both carbon and oxygen atoms are bound to the metal center. Isolated η^2-acyl complexes are very reactive and readily undergo a variety of interesting transformations,[3] such as deinsertion, the insertion of the alkyl group into the acyl moiety to generate an η^2-ketone,[9] or the uptake of a second CO molecule to give an enediolate.[10]

Isocyanides typically insert into early transition metal-carbon bonds producing η^2-iminoacyl functionalities.[2,3,11] The insertion of isocyanides into early transition metal−alkyl bonds has been extensively studied in recent years because the resulting η^2-iminoacyl compounds are much more accessible and less reactive than the related η^2-acyl derivatives. Analogously to η^2-acyl complexes, η^2-iminoacyls undergo insertion of the alkyl group into the iminoacyl moiety, to generate an η^2-imine, or the uptake of a second isocyanide molecule, to give an enediamide.[3,11,12] However, unlike carbon monoxide, isocyanides hardly undergo deinsertion but rather may easily give rise to multiple insertion into various metal−carbon bonds, providing useful synthetic

(1) Kulhmann, E. J.; Alexander, J. J. *Coord. Chem. Rev.* **1980**, it 33, 195.
(2) Alexander, J. J. In *The Chemistry of the Metal−Carbon Bond*; Hartley, F. R., Ed.; Wiley: New York, 1985; Vol. 2.
(3) Durfee, L. D.; Rothwell, I. P. *Chem. Rev.* **1988**, *88*, 1059.
(4) Wojcicki, A. *Adv. Organomet. Chem.* **1973**, *11*, 97.
(5) Foold, T. C. In *Topics in Stereochemistry*; Geoffry, G. L., Ed.; Wiley: New York, 1981; Vol. 12, p 83.
(6) Wax, M. J.; Bergman, R. G. *J. Am. Chem. Soc.* **1981**, *103*, 7028.
(7) Lauher, J. W.; Hoffmann, R. *J. Am. Chem. Soc.* **1976**, *98*, 1729; Tatsumi, K.; Nakamura, A.; Hofmann, P.; Stauffert, P.; Hoffmann, R. *J. Am. Chem. Soc.* **1985**, *107*, 4440. Hofmann, P.; Stauffert, P.; Tatsumi, K.; Nakamura, A.; Hoffmann, R. *Organometallics* **1985**, *4*, 404.
(8) Berke, H.; Hoffmann, R. *J. Am. Chem. Soc.* **1978**, *100*, 7224.
(9) Erker, G.; Rosenfeldt, F. *J. Organomet. Chem.* **1982**, *224*, 29−42.
(10) Manriquez, J. M.; McAlister, D. R.; Sanner, R. D.; Bercaw, J. E. *J. Am. Chem. Soc.* **1978**, *100*, 2716. Hofmann, P.; Stauffert, P.; Frede, M.; Tatsumi, K. *Chem. Ber.* **1989**, *122*, 1559.
(11) Chamberlain, R. L.; Durfee, L. D.; Fanwick, P. E.; Kobriger, R.; Latesky, S. L.; McMullen, A. K.; Rothwell, I. P.; Folting, K.; Huffman, J. C.; Streib, W. E.; Wang, R. *J. Am. Chem. Soc.* **1987**, *109*, 390.
(12) Chamberlain, R. L.; Durfee, L. D.; Fanwick, P. E.; Kobriger, R.; Latesky, S. L.; McMullen, A. K.; Steffey, B. D.; Rothwell, I. P.; Folting, K.; Huffman, J. C. *J. Am. Chem. Soc.* **1987**, *109*, 6068.

10.1021/om020250j CCC: $22.00 © 2002 American Chemical Society
Publication on Web 08/28/2002

Scheme 1

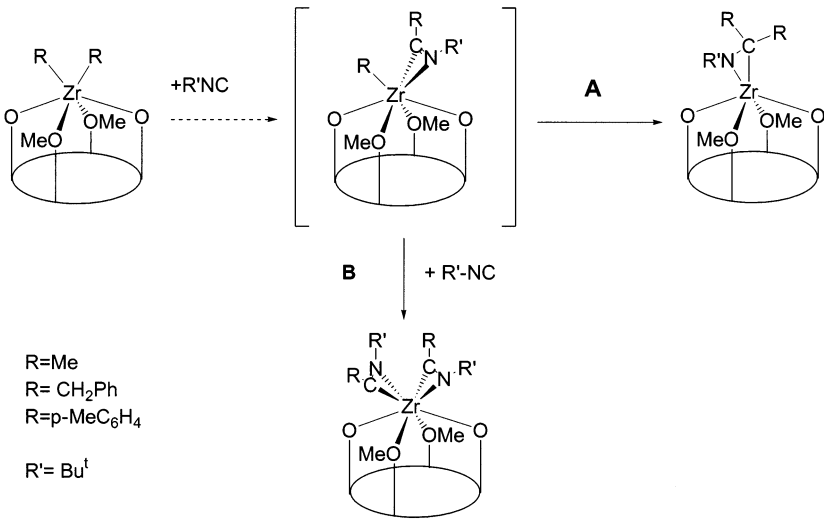

Downloaded by CARLI CONSORTIUM on June 29, 2009
Published on August 28, 2002 on http://pubs.acs.org | doi: 10.1021/om020250j

routes to nitrogen-containing organic compounds.[3] Moreover, while further insertion of CO into the metal−carbon bond of η^2-acyl compounds is less known, insertion of isocyanides into metal−iminoacyl bonds has been observed, and many examples of the double insertion of isocyanides into the metal−carbon bond of η^2-iminoacyl ligands have been reported.[3,13]

Recently, it has been reported the multistep migratory insertion of several isocyanides into the metal−carbon bonds of the ZrR_2 fragment anchored to a tetraoxo matrix, defined by the dimethoxycalix[4]arene dianion [*p*-Bu^t-calix[4](OMe)$_2$(O)$_2$]$^{2-}$.[14] The reaction of this complex with isocyanides testifies to the migratory aptitude of the methyl groups bound to the zirconium center. The reaction of [*p*-Bu^t-calix[4](OMe)$_2$(O)$_2$ZrR$_2$] (**1**, R = Me, CH_2Ph, *p*-MeC_6H_4) with Bu^{t}NC shows two different migratory insertion pathways depending on temperature, see Scheme 1. The reaction of **1** with Bu^{t}NC at room temperature with a 1:1 Zr/Bu^{t}NC molar ratio leads only to the η^2-imine complex, via the intermediacy of the corresponding methyl-η^2-iminoacyl species, path A in Scheme 1. On the other hand, at low temperature the reaction shows the preferential migration of the second alkyl group to an incoming Bu^{t}NC, to give a bis-η^2-iminoacyl, regardless of the Zr/Bu^{t}NC stoichiometric ratio, path B in Scheme 1.

Relevant differences have been observed between the reaction of [*p*-Bu^t-calix[4](OMe)$_2$(O)$_2$Zr(Me)$_2$] with Bu^{t}NC and that with CO.[14] Unlike the reaction of **1** with Bu^{t}NC, that with CO proceeds via a two-step migration to give directly the corresponding η^2-acetone [*p*-Bu^t-calix[4](OMe)$_2$(O)$_2$Zr(Me$_2$CO)]. Although the formation of the η^2-acetone was theoretically shown to occur via the intermediacy of an η^2-acyl species,[15] such a species is too reactive and could not be experimentally intercepted, at variance with the isocyanide reaction where a bis-η^2-iminoacyl complex was isolated and structurally characterized.[14]

In the present study we investigate the multistep isocyanide insertion into the zirconium−alkyl bond in [*p*-Bu^t-calix[4](OMe)$_2$(O)$_2$ZrMe$_2$] combining "static" DFT calculations on the stationary points of the potential surface with ab initio molecular dynamics simulations (AIMD) based on the Car−Parrinello approach.[16] Gradient-corrected DFT calculations have been performed to compute the geometries and the relative stabilities of the stationary points of the potential energy surface for both paths A and B. Transition states for the key steps of both considered pathways have been localized. Car−Parrinello simulations have been employed to study the detailed dynamic features of (i) the isocyanide migratory insertion from the [calix[4](OMe)$_2$(O)$_2$ZrMe$_2$](CNMe) adduct to the η^2-iminoacyl complex, (ii) the subsequent methyl to iminoacyl migration from the [calix[4](OMe)$_2$-(O)$_2$ZrMe(η^2-MeCNMe)] iminoacyl complex, leading to the η^2-imine moiety, and (iii) the second isocyanide migratory insertion from the [calix[4](OMe)$_2$(O)$_2$ZrMe-(η^2-MeCNMe)] iminoacyl complex leading to the corresponding bis-η^2-iminoacyl complex.

Computational Details

We model the [*p*-Bu^t-calix[4](OMe)$_2$(O)$_2$] ligand by replacing the Bu^t para substituents by H atoms; it has been shown that for this class of compounds this approximation does not affect the electronic properties of the investigated systems.[17] Also, the Bu^t-CN group was modeled by MeNC.

Static DFT Calculations. All the static DFT calculations reported in this paper are based on the ADF (Amsterdam Density Functional) program package described elsewhere.[18,19] The frozen cores have been 1s−4p for Zr and 1s for C and O. The molecular orbitals were expanded in an uncontracted DZ STO basis set for all atoms with the exception of the transition metal orbitals for which we used a DZ STO basis set for *n*s and *n*p and a TZ STO basis set for *n*d and (*n*+1)s. As polarization functions, one 5p, one 3d, and one 2p STO were

(13) Moloy, K. G.; Fagan, P. J.; Manriquez, J. M.; Marks, T. J. *J. Am. Chem. Soc.* **1986**, *108*, 56.
(14) Giannini, L.; Caselli, A.; Solari, E.; Floriani, C.; Chiesi-Villa, A.; Rizzoli, C.; Re, N.; Sgamellotti, A. *J. Am. Chem. Soc.* **1997**, *119*, 9709.
(15) Fantacci, S.; De Angelis, F.; Sgamellotti, A.; Re, N. *Organometallics* **2001**, *20*, 4031.
(16) Car, R.; Parrinello, M. *Phys. Rev. Lett.* **1985**, *55*, 2471.
(17) Fantacci, S.; Sgamellotti, A.; Re, N.; Floriani, C. *J. Chem. Soc., Dalton Trans.* **2001**, 1718.
(18) Ziegler, T.; Tshinke, V.; Baerends, E. J.; Snijders, J. G.; Ravenek, W.; *J. Phys. Chem.* **1989**, *93*, 3050.
(19) (a) Baerends, E. J.; Ellis, D. E.; Ros, P. *Chem. Phys.* **1973**, *2*, 42. (b) Baerends, E. J.; Ros, P. *Chem. Phys.* **1973** 2, 51. (c) Baerends, E. J.; Ros, P. *Chem. Phys.* **1975**, 8, 41. (d) Baerends, E. J.; Ros, P. *Int. J. Quantum Chem.* **1978**, *S12*, 169.

used for Zr, O, N and C, and H, respectively. Geometry optimizations were performed without any symmetry constraints, using the Vosko−Wilk−Nusair LDA parametrization[20] and including the Becke[21] and Perdew−Wang[22] gradient corrections to the exchange and correlation, respectively. Transition states were located by using the Powell method[23] implemented in the ADF package. Due to the large size of the investigated systems, no frequency calculations were performed on the optimized structures. Therefore we refer to transition state structures which have one negative eigenvalue of the approximate Hessian matrix.

Car−Parrinello Calculations. AIMD simulations were carried out with the Car−Parrinello (CP) method.[16,24,25] For the LDA exchange-correlation functional the Perdew−Zunger parametrization[26] has been used, while the gradient-corrected functional is taken from ref 27. Core states are projected out by using pseudopotentials. For Zr, C, O, and H "ultra-soft" pseudopotentials were generated according to the scheme proposed by Vanderbilt.[25] The wave functions were expanded in plane waves up to an energy cutoff of 25 Ry. Periodic boundary conditions were used by placing the model molecule in a cubic box of 15.87 Å, keeping a minimum of 6.0 Å between repeated images, sufficiently large to avoid any coupling between periodic images. The equations of motion were integrated by using a time step of 10 au (0.242 fs) with an electronic fictitious mass $\mu = 1000$ au. Constrained AIMD simulations were performed by means of the SHAKE algorithm,[28] employing the slow-growth method[29] in which the constrained parameter is slowly varied as a function of the simulation time, in such a way that the potential energy surface along the considered constraint is dynamically sampled; to maintain the system in thermal equilibrium the temperature of the nuclei was controlled by a Nosé thermostat,[30] which creates a canonical (NVT) ensemble. All simulations were conducted at 300 K. To obtain a thermal distribution of vibrational modes, the temperature was gradually increased by small steps.

The consistency of the CP and ADF programs already has been checked in ref 15 comparing the geometries of the fully optimized [calix[4](OMe)$_2$(O)$_2$Zr(Me)$_2$] complex **1** with the analogous [*p*-Bu^t-calix[4](OMe)$_2$(O)$_2$Zr(CH$_2$Ph)$_2$] complex, for which X-ray data are available.[14]

Results and Discussion

Both pathways A and B in Scheme 1 are supposed to be initialized by the isocyanide migratory insertion leading to an η^2-iminoacyl complex. We therefore start our analysis by investigating the first step of isocyanide insertion, i.e., the coordination of MeNC at the zirconium center of [calix[4](OMe)$_2$(O)$_2$Zr(Me)$_2$], see Scheme 1. We optimized the geometry of complex **1** under C_{2v} symmetry constraints[15] with the two methyl carbon atoms bound to zirconium lying in the *yz* plane, see Figure 1 and Table 1. Hereafter we will refer to C_α and C_β as respectively the carbon of the methyl group undergoing the MeNC insertion and the remaining methyl carbon, O_1 and O_3 as the phenoxo oxygens, and O_2 and O_4 as the methoxy oxygens.

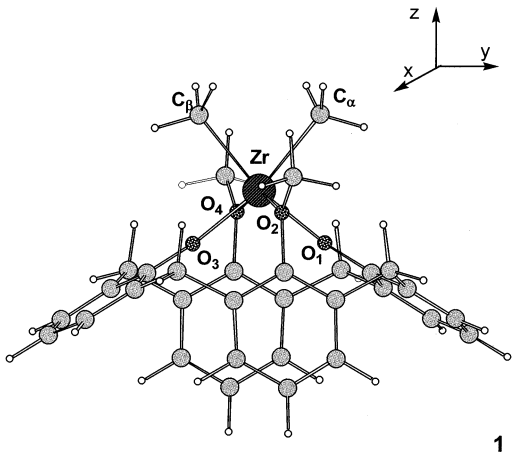

1

Figure 1. Optimized geometrical structure of the [calix-[4](OMe)$_2$(O)$_2$ZrMe$_2$] complex **1**.

Table 1. Optimized Geometrical Parameters (bond lengths in Å and angles in deg) of [*p*-Bu^t-calix[4](OMe)$_2$(O)$_2$ZrMe$_2$] (1), MeNC Adduct 2, η^1-Iminoacyl Complex 3b, and η^2-Iminoacyl Complex 3a

parameters	1	2	3b	3a
R_{Zr-O_1}	2.060	2.063	2.027	2.066
R_{Zr-O_2}	2.389	2.484	2.399	2.433
R_{Zr-O_3}	2.060	2.057	2.015	2.052
R_{Zr-O_4}	2.389	2.574	2.504	2.430
R_{Zr-C_α}	2.336	2.402	3.070	
R_{Zr-C_β}	2.336	2.389	2.310	2.342
R_{Zr-CN}		2.270	2.308	2.280
R_{Zr-N}				2.270
R_{C-N}		1.180	1.283	1.279
$R_{C_\alpha-CN}$		2.510	1.537	1.496
$R_{C_\beta-CN}$		2.645	2.742	3.034
$\angle O_1ZrO_3$	104.7	106.2	120.7	103.3
$\angle O_2ZrO_4$	154.5	147.6	154.0	150.0
$\angle C_\alpha CZr$		60.1	104.2	159.7
$\angle CZrC_\beta$		69.1	72.8	82.0
$\angle ZrCN$		177.5	132.5	73.2
$\angle NCZrC_\beta$		62.7	83.8	89.0

Frontier orbital analysis performed on complex **1**[15] revealed an isolated LUMO of essentially zirconium d_{xz} character, which represents the only vacant molecular orbital to which the incoming nucleophilic ligand can donate prior to insertion. Moreover, previous extended Hückel calculations on the [calix[4](OMe)$_2$(O)$_2$Zr]$^{2+}$ fragment have shown four non-coplanar low-lying metal orbitals, $1a_1(d_{z^2})$, $1b_1(d_{xz})$, $1b_2(d_{yz})$, and $1a_2(d_{xy})$, which favor a facial geometry of the three additional L ligands of a [calix[4](OMe)$_2$(O)$_2$ZrL$_3$] species.[14] Because of the spatial extension of the LUMO and the peculiar electronic structure of complex **1** we expect that the most favorable approach of MeNC occurs along a line in the plane bisecting the Me−Zr−Me angle (*xz*) forming an angle of ca. 45° with the *z* axis, leading to a facial adduct, the same coordination mode already found for CO in ref 15. To check this point we optimized the geometry of the MeNC adduct without any symmetry constraints, finding a facial structure, **2**, shown in Figure 2, consistent with the frontier orbital picture exposed above. The optimized geometry, see Table 1,

(20) Vosko, S. H.; Wilk, L.; Nusair, M. *Can. J. Phys.* **1980**, *58*, 1200.
(21) Becke, A. D. *Phys. Rev.* **1988**, *A38*, 3098.
(22) Perdew, J. P.; Wang, Y. *Phys. Rev.* **1992**, *B45*, 13244.
(23) Powell, M. J. D. *Math. Prog.* **1977**, *12*, 241.
(24) The implementation that we use is decribed in: Pasquarello, A.; Laasonen, K.; Car, R.; Lee, C.; Vanderbilt, D. *Phys. Rev. Lett.* **1992**, *69*, 1982. Pasquarello, A.; Laasonen, K.; Car, R.; Lee, C.; Vanderbilt, D. *Phys. Rev. B* **1993**, *47*, 10142.
(25) Vanderbilt, D. *Phys. Rev. B* **1990**, *41*, 7892.
(26) Perdew, J. P.; Zunger, A. *Phys. Rev. B* **1981**, *23*, 5048.
(27) Perdew, J. P.; Chevary, J. A.; Vosko, S. H.; Jackson, K. A.; Pederson, M. R.; Singh, D. J.; Fiolhais, C. *Phys. Rev. B* **1992**, *46*, 6671.
(28) Ryckaert, J.-P.; Ciccotti, G.; Berendsen, H. J. *J. Comput. Phys.* **1977**, *23*, 327.
(29) Straatsma, T. P.; Berendsen, H. J. C.; Postma, J. P. M. *J. Chem. Phys.* **1986**, *85*, 6720.
(30) Nosé, S. *Mol. Phys.* **1984**, *52*, 255. Hoover, W. G. *Phys. Rev. A* **1985**, *31*, 1695.

Downloaded by CARLI CONSORTIUM on June 29, 2009
Published on August 28, 2002 on http://pubs.acs.org | doi: 10.1021/om020250j

Downloaded by CARLI CONSORTIUM on June 29, 2009
Published on August 28, 2002 on http://pubs.acs.org | doi: 10.1021/om020250j

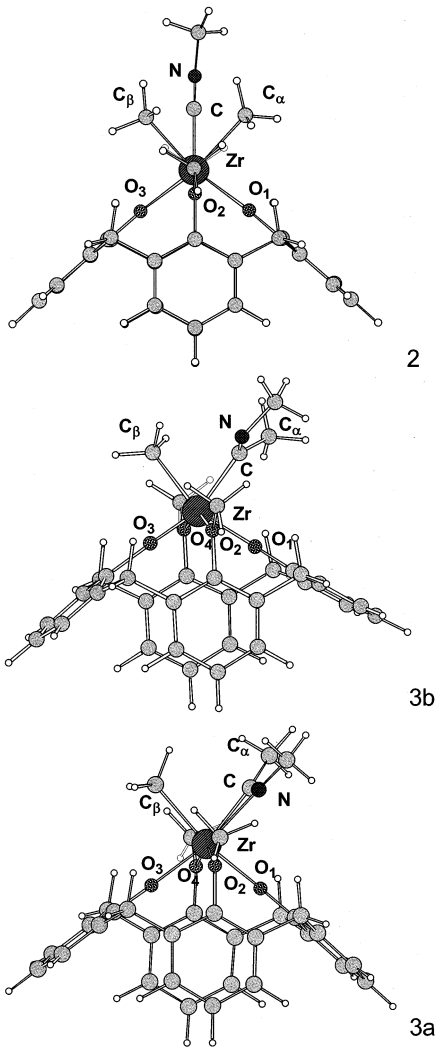

Figure 2. Optimized geometrical structures of the MeNC adduct **2**, η^2-iminoacyl, **3a**, and η^1-iminoacyl, **3b**, complexes.

reflects the geometrical perturbation due to the coordination of MeNC which prepares the insertion reaction. The resulting $Zr-C_{\alpha,\beta}$ bond lengths are ca. 0.5−0.7 Å longer than in the dimethyl complex **1**, as well as the $Zr-O_{2,4}$ distances, which are ca. 0.1−0.2 Å longer. The Zr−C(CNMe) distance is quite long, 2.270 Å, reflecting a weak interaction between the MeNC ligand and the $[calix[4](OMe)_2(O)_2ZrMe_2]$ fragment, as expected since the MeNC ligand cannot exploit any stabilizing π back-donation interaction with a d^0 electron deficient metal center such as Zr(IV). Complex **2** was found 9.4 kcal mol^{-1} (5.0 kcal mol^{-1} when accounting for BSSE correction) more stable than the reagents (dimethyl complex **1** + MeNC). To check whether a barrier to MeNC coordination exists, we optimized the transition state structure relative to MeNC coordination, $\mathbf{TS}_{1\rightarrow 2}$, finding an energy barrier of 5.5 kcal mol^{-1} (with respect to the BSSE corrected sum of the energies of the free reagents), corresponding to a Zr−C(CNMe) distance of 3.433 Å. This barrier is higher than that computed for CO coordination (<2.0 kcal mol^{-1}),[15] probably reflecting the larger steric hindrance of the isocyanide species.

To understand the mechanism of the isocyanide migratory insertion in the $[calix[4](OMe)_2(O)_2ZrMe_2]$-(CNMe) adduct, we carried out dynamics simulations on complex **2**. We started the dynamics simulation by heating the structure of the MeNC adduct **2** in the geometry obtained by the static DFT optimization. We did not apply any constraints to the molecular motion, allowing all the degrees of freedom to evolve naturally in time. The total time span of the simulation was 2.5 ps. The MeNC migratory insertion can be followed by studying the time evolution of several geometrical parameters, such as the C_α−C(CNMe) distance, the Zr−C_α(Me) distance, and the Zr−N distance.

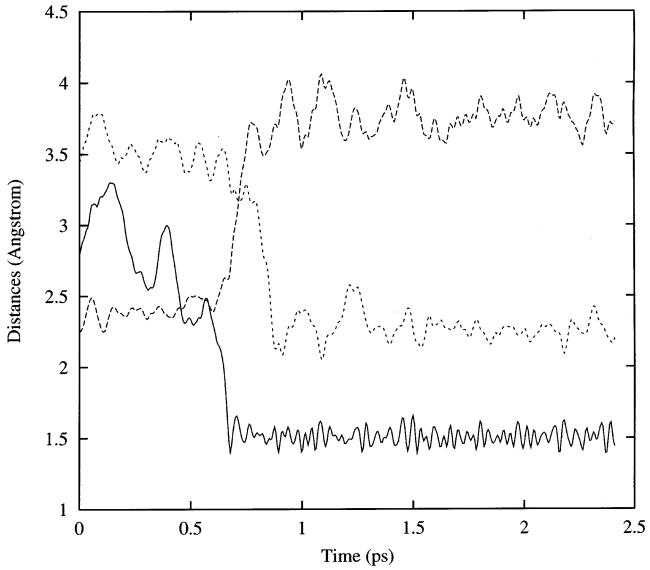

Figure 3. Time evolution of the C_α−C (solid line), Zr−C_α (dashed line), and Zr−N (dotted line) distances for the entire time span going from 0 to 2.5 ps, for the first isocyanide migratory insertion from adduct **2** to the η^2-iminoacyl complex **3b**. Time in ps and distances in Å.

Figure 3 displays the variation of the C_α−C, Zr−C_α, and Zr−N distances as a function of the simulation time and clearly shows that the reactive MeNC migration takes place within ca. 0.6 ps, as testified by the fast decrease in the C_α−C distance from ca. 2.6 Å to ca. 1.5 Å. Thereafter, this parameter varies within the normal limits of a carbon−carbon bond vibration. At the same time the Zr−C_α distance follows an almost complementary trajectory with respect to the C_α−C distance and grows from ca. 2.5 Å up to ca. 3.7 Å, reflecting the methyl detachment from the metal center upon MeNC insertion. However, this parameter shows higher oscillations after 0.7 ps, since the Zr and CH_3 groups are no longer bound at the end of the reaction. The Zr−N distance is found to decrease from its initial value, ca. 3.5 Å, to ca. 2.2 Å, corresponding to a Zr−N bond in an η^2-iminoacyl species, **3a**, within 0.9 ps. It is worth noting that the formation of the Zr−N bond is delayed by ca. 0.3 ps with respect to the C_α−C bond formation, suggesting the initial formation, after 0.6 ps, of a transient η^1-iminoacyl species, **3b**, with a formed C_α−C bond and still a long Zr−N bond. The short time stability of the η^1-iminoacyl species (ca. 0.3 ps) suggests a negligible barrier for the conversion of the η^1- into the η^2-isomer, the same result already found for CO insertion in bis-(cyclopentadienyl)[31] and calix[4]arenes[15] Zr dimethyl complexes. Interestingly, the migratory insertion reac-

(31) De Angelis, F.; Re, N.; Sgamellotti, N. *Organometallics* **2000**, *19*, 4904. De Angelis, F.; Re, N.; Sgamellotti, N. *Organometallics* **2001**, *20*, 1486.

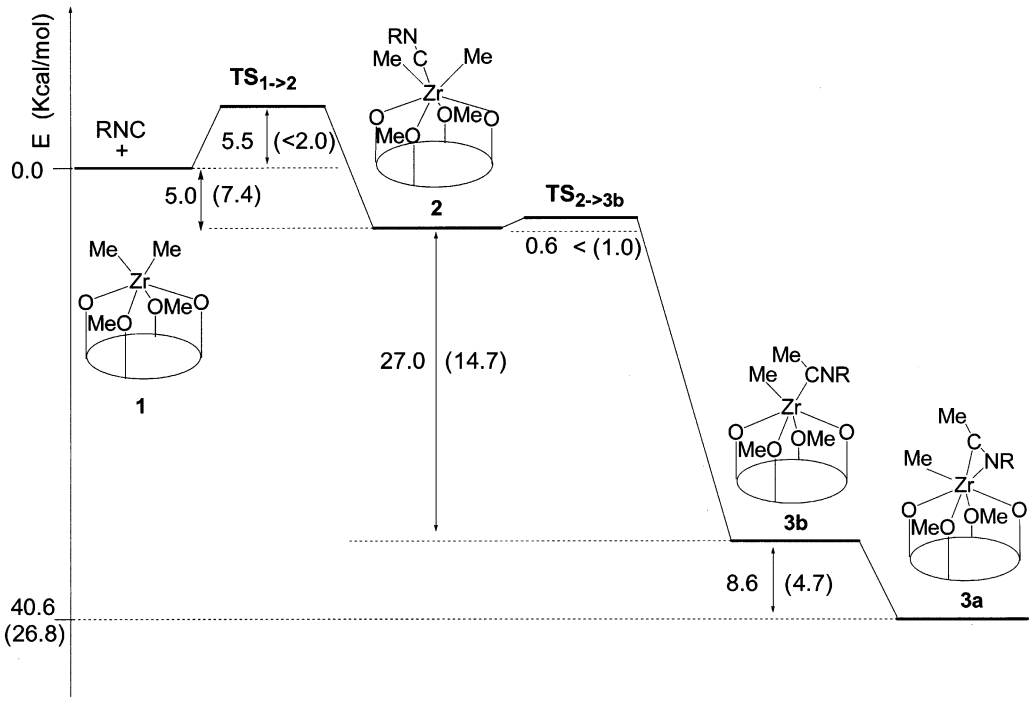

Figure 4. Schematic representation of the potential energy surface for the MeNC coordination and insertion into the Zr−Me bond. The zero of the energy corresponds to the BSSE corrected sum of the energies of the free reagents. The values in parentheses refer to the energies computed for CO migratory insertion.[15] Energy in kcal mol^{-1}.

Downloaded by CARLI CONSORTIUM on June 29, 2009
Published on August 28, 2002 on http://pubs.acs.org | doi: 10.1021/om020250j

tion seems to occur by an isocyanide insertion into the Zr−Me bond rather than by a methyl attack to the resting isocyanide group; indeed, the time evolution of the $\angle O_2-Zr-C_\alpha-C_\beta$ dihedral angle shows almost constant oscillations around ca. 90° up to ca. 0.9 ps, while the $\angle C-Zr-O_2-C_\alpha$ dihedral angle decreases from ca. 140° to ca. 100° within 0.7 ps, reflecting the isocyanide approach to the methyl prior to the $C_\alpha-C$ bond formation (see Figure S1 in the Supporting Information).

Dynamics simulations have shown that the final product of isocyanide insertion into the Zr−Me is the η^2-iminoacyl species **3a**, confirming the intermediacy of such a species postulated in ref 14. We therefore optimized the geometry of the η^2- (**3a**) and η^1- (**3b**) iminoacyl isomers without any symmetry constraints, finding two structures with the CN group lying almost perpendicular to the *yz* plane, as shown in Figure 2. Geometrical parameters of complexes **3a** and **3b** are reported in Table 1; it is worth noting that our calculations reproduce quite faithfully the peculiar flexibility of the calixarene ligand that rearranges on the basis of the two different coordination modes; indeed, the $\angle O_1ZrO_3$ and $\angle O_2ZrO_4$ angles are close in the η^2-iminoacyl complex by ca. 17° and ca. 4° with respect to the corresponding values in the η^1-isomer. Both the η^1- and the η^2-bound iminoacyls are found to be much more stable than the facial adduct **2**, by 27.0 and 35.6 kcal mol^{-1}, respectively. We then optimized the transition state structure for the isocyanide insertion into the Zr−Me bond, $\mathbf{TS}_{2\rightarrow 3b}$, finding a barrier of only 0.6 kcal mol^{-1} comparable to the value already computed for CO insertion. Therefore, the different reactivity of the inserting CO and MeNC groups seems to be driven by the much higher exothermicity computed for formation of the η^2-iminoacyl with respect to the corresponding η^2-acyl species (35.6 vs 19.4 kcal mol^{-1}), consistent with the experimental evidence that isocyanide deinsertion is an extremely rare process at variance with CO deinsertion. A summary of the energetics for MeNC coordination and migration has been reported in Figure 4, along with the corresponding data obtained for CO migration (in parentheses), for a direct comparison.

1. Reactivity of η^2-Iminoacyls. The initially formed methyl-η^2-iminoacyl complex **3a** can undergo two competitive reactive pathways: (i) the methyl-to-iminoacyl migration, leading to an η^2-bound imine, path A in Scheme 1, and (ii) the uptake of a second isocyanide molecule and its insertion into the residual $Zr-CH_3$ bond to give a bis-η^2-iminoacyl complex, path B in Scheme 1.

1.a Path A. We optimized the structure of the [calix[4](OMe)$_2$(O)$_2$Zr(η^2-N(Me)C(Me)$_2$)] imine complex **4**, finding a structure 12.2 kcal mol^{-1} more stable than the η^2-iminoacyl **3a**, and thoroughly 52.8 kcal mol^{-1} lower than the starting reagents. The lower exothermicity computed for formation of **4** with respect to formation of the corresponding ketone complex (12.2 vs 41.1 kcal mol^{-1}) reflects the less effective π back-donation in the former complex, due to the higher energy of the π^* orbital of the iminoacyl with respect to that of the acyl species, vide infra. The optimized structure is shown in Figure 5 and the main computed geometrical parameters are presented in Table 2 together with the X-ray data for the [*p*-Bu^t-calix[4](OMe)$_2$(O)$_2$Zr(η^2-N(Bu^t)-C(CH$_2$Ph)$_2$)] complex, the closest structurally characterized compound. The optimized structure of complex **4** is in good agreement with the experimental data and reproduces the calix[4]arene moiety deviation from the peculiar cone conformation as a function of the different coordination modes of the metal, with the two methoxy-bearing phenyl rings oriented toward the macrocyclic cavity and the phenoxo rings pushed outward, see Figure 5. Slight discrepancies are observed for the $Zr-O_{2,4}$ bond distances (respectively 0.063 and 0.072 Å

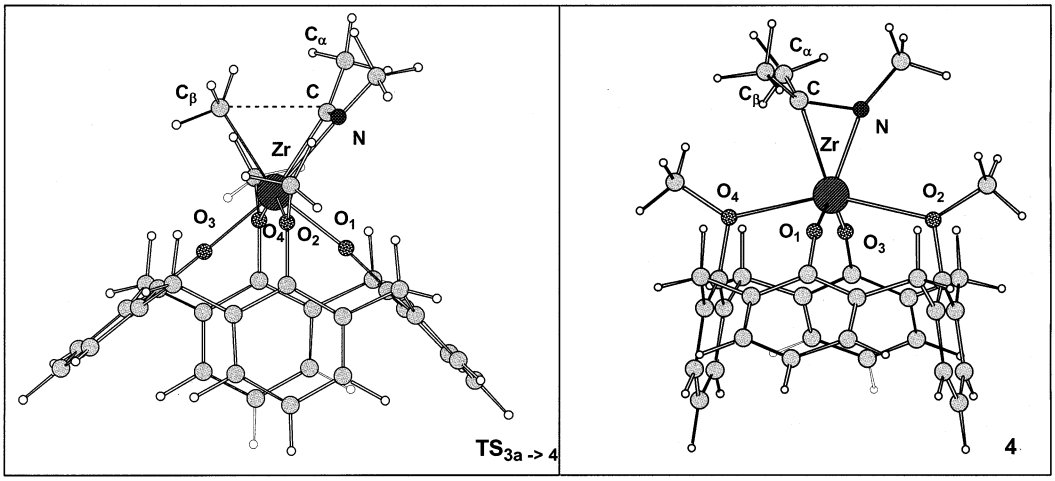

Figure 5. Optimized geometrical structures of the transition states for imine formation, $\mathbf{TS}_{3a\rightarrow4}$, and of η^2-imine complex **4**.

Table 2: Optimized Geometrical Parameters (bond lengths in Å and angles in deg) of the Transition State for the Formation of η^2-Imine, $TS_{3a\rightarrow4}$, and of the η^2-Imine Complex 4, Compared to X-ray Data for the [*p*-Bu^t-calix[4](OMe)$_2$(O)$_2$ZrN(Bu^t)C(CH$_2$Ph)$_2$] Complex[14]

parameters	$\mathbf{TS}_{3a\rightarrow4}$	**4**	exptl [ref 14]
R_{Zr-O_1}	2.051	2.040	1.963(6)
R_{Zr-O_2}	2.415	2.433	2.496(6)
R_{Zr-O_3}	2.061	2.047	2.023(5)
R_{Zr-O_4}	2.425	2.419	2.347(5)
R_{Zr-C_β}	2.365	3.331	
R_{Zr-CN}	2.241	2.244	2.271(8)
R_{Zr-N}	2.279	2.043	2.045(7)
R_{C-N}	1.287	1.430	1.429(10)
$R_{C_\alpha-CN}$	1.493	1.540	
$R_{C_\beta-CN}$	2.763	1.562	
$\angle O_1ZrO_3$	102.7	132.3	120.3(2)
$\angle O_2ZrO_4$	149.2	154.5	150.2(2)
$\angle C_\alpha CZr$	158.5	120.4	
$\angle CZrC_\beta$	73.7	23.7	
$\angle ZrCN$	75.1	63.1	62.3(4)
$\angle NCZrC_\beta$	111.9	104.1	

longer than the experimental values) and can be related to the weak interaction between the etheric oxygens and the zirconium center; the $\angle O_1ZrO_3$ is computed to be 12.0° larger than the experimental value reflecting the presence of bulky benzyl groups in the experimentally characterized compound.

To cast some light onto the reaction mechanism of the methyl migration, we performed constrained dynamics simulations starting from complex **3a**; the total time span of the simulation was 3.0 ps. The results have been interpreted in terms of the time evolution of the $Zr-C_\beta$ and N−C distances, and of the $\angle NCZrC_\beta$ dihedral angle (see Figures S2 and S3, respectively, in the Supporting Information). Methyl migration was found to take place for a value of the RC close to 1.9 Å, corresponding to 2.2 ps; since the $\angle NCZrC_\beta$ dihedral angle, which characterizes the orientation of the iminoacyl group with respect to the inserting methyl, oscillates between 60° and 120° and no variations in this parameter are observed in correspondence of methyl migration (2.2 ps), we conclude that the methyl attack occurs almost perpendicularly to the iminoacyl plane.

Indeed, extracting selected configurations from the dynamics simulation, we were able to locate the transition state connecting **3a** and **4**, $\mathbf{TS}_{3a\rightarrow4}$, finding a structure (see Figure 5 and Table 2) with a $C_\beta-CN$ distance of 2.763 Å, i.e., 0.271 Å shorter than in **3a**, which corresponds to a closure of the $\angle CZrC_\beta$ of 8.3°. The methyl attack is favored to occur quasiorthogonally to the C−N plane, as indicated by the $\angle NCZrC_\beta$ dihedral angle of 111.9° in $\mathbf{TS}_{3a\rightarrow4}$, because of the presence of a low-lying LUMO of mainly π^*_{CN} character oriented perpendicular to the iminoacyl plane, see Figure 6, which is responsible of the electrophilic character of the iminoacyl carbon toward the residual methyl attack. The resulting energy barrier is found to be 6.4 kcal mol^{-1}, i.e., 4.1 kcal mol^{-1} higher than that computed for the η^2-ketone formation.[15] Such a difference can be related to electronic factors, indeed, the iminoacyl LUMO, the π^*_{CN} orbital, has a higher energy than that of the π^*_{CO} orbital in the corresponding acyl complex (−2.01 vs −2.43 kcal mol^{-1}),[15] contributing to making the methyl-to-iminoacyl migration more difficult. A schematic representation of the potential energy surface for path A has been reported in Figure 7.

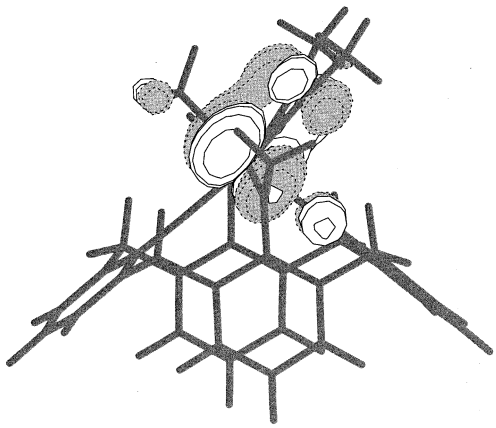

Figure 6. Isodensity surface plot of the LUMO orbital of the [calix[4](OMe)$_2$(O)$_2$Zr(Me)(η^2-CNMe)] iminoacyl complex **3b**. Contour value 0.04.

1.b. Path B. We now investigate the uptake of a second isocyanide followed by its insertion into the $Zr-C_\beta H_3$ bond of complex **3a**, leading to a bis-η^2-iminoacyl species. For the sake of clearness hereafter we indicate the carbon and nitrogen of the coordinated

Downloaded by CARLI CONSORTIUM on June 29, 2009
Published on August 28, 2002 on http://pubs.acs.org | doi: 10.1021/om020250j

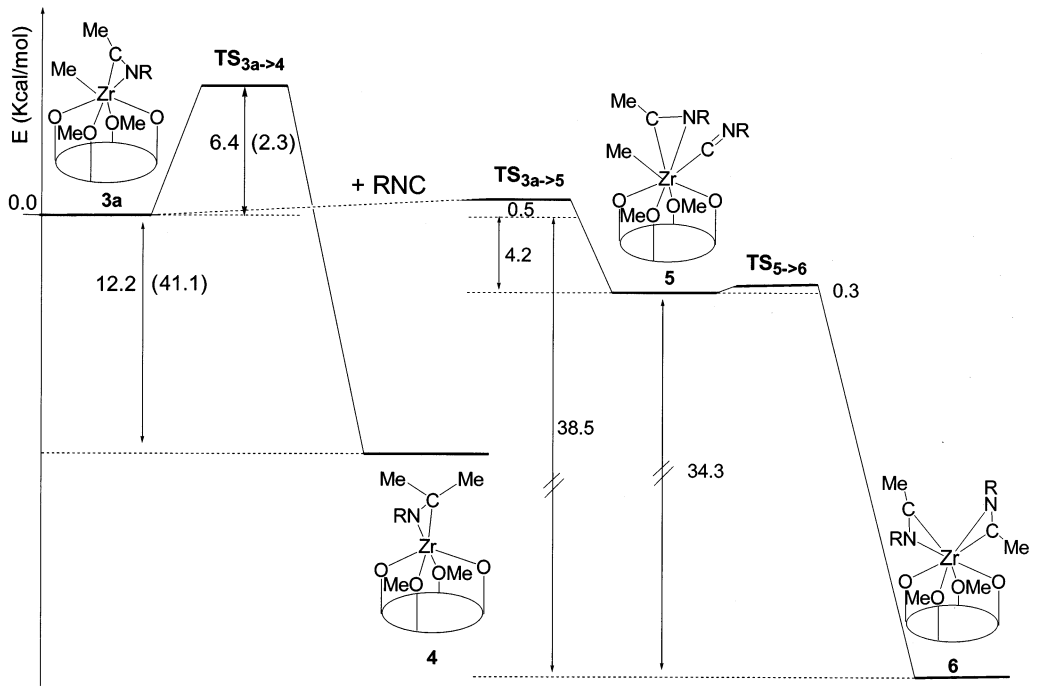

Figure 7. Schematic representation of the potential energy surface of methyl to iminoacyl migration, path A, and insertion of a second methyl isocyanide into the $Zr-CH_3$ bond, path B. The zero of the energy of the intermolecular path B corresponds to the BSSE corrected sum of the energies of the free reagents. The values in parentheses refer to the energy computed for the corresponding methyl-to-acyl migration.[15] Energy in kcal mol^{-1}.

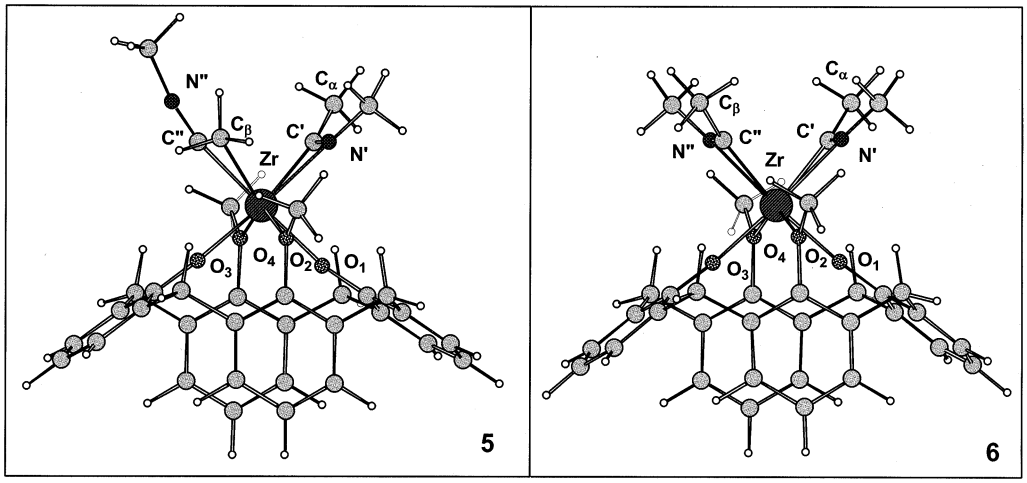

Figure 8. Optimized geometrical structure of the MeNC adduct **5** and of the bis-η^2-iminoacyl complex **6**.

iminoacyl as C′ and N′, and the carbon and nitrogen of the incoming isocyanide as C″ and N″. Since in this case also the insertion reaction is preceded by the isocyanide coordination, we checked the presence of an energy barrier to C″N″−Me coordination by optimizing the relative transition state structure. We computed a barrier of only 0.5 kcal mol^{-1} (with respect to the BSSE corrected sum of the energies of the free reagents), corresponding to a Zr−C″ distance of 3.290 Å. We then optimized the geometry of the resulting adduct, complex **5**, see Figure 8, finding a structure 8.0 kcal mol^{-1} (4.2 kcal mol^{-1} when accounting for BSSE correction) below the starting reagents, see Figure 7.

To cast some light into the second insertion reaction mechanism, dynamics simulations were performed starting from complex **5**. We therefore heated the structure of the isocyanide adduct **5** in the geometry obtained by the static DFT optimization. In this case too, we did not apply any constraints to the molecular motion, allowing all the degrees of freedom to evolve naturally for a total time of 2.5 ps. The second isocyanide migratory insertion can be followed by studying the time evolution of the geometrical parameters already analyzed in the first isocyanide insertion, i.e., the $C_\beta-C''$ distance, the $Zr-C_\beta$(Me) distance, and the Zr−N″ distance. The results, reported in Figure 9, are quite similar to those observed for the first MeNC insertion, and will not therefore be discussed in detail. It is sufficient to note that in this case the migratory insertion leads to a bis-$\eta^1\eta^2$-bound iminoacyl as a preliminary product, which relaxes into the corresponding bis- $\eta^2\eta^2$-bound isomer within 0.4 ps, as shown by the delay of ca. 0.3 ps in the formation of the $C_\beta-C''$ bond and the coordination of N″ to the Zr center.

We finally optimized the geometry of the bis-η^2-iminoacyl complex, **6**, finding the same head-to-tail

Downloaded by CARLI CONSORTIUM on June 29, 2009
Published on August 28, 2002 on http://pubs.acs.org | doi: 10.1021/om020250j

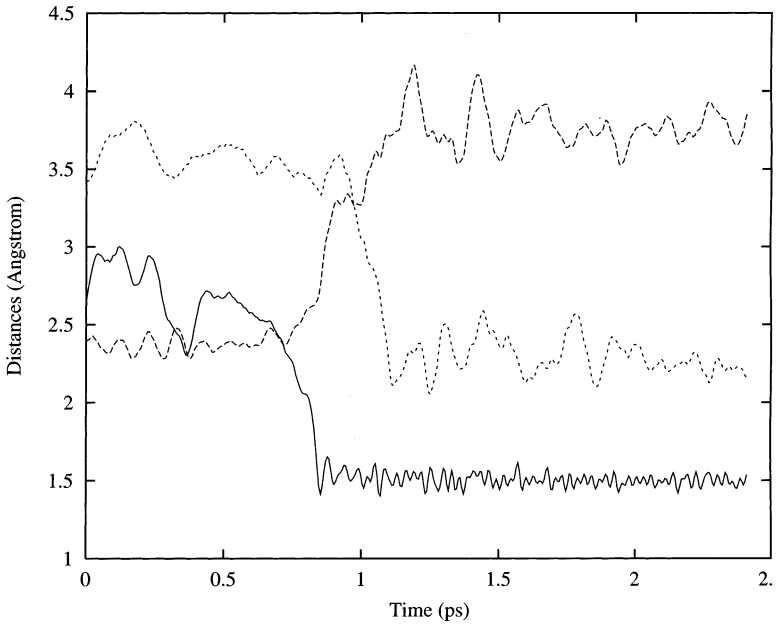

Figure 9. Time evolution of the $C_\beta-C''$ (solid line), $Zr-C_\beta(Me)$ (dashed line), and $Zr-N''$ (dotted line) distances for the entire time span going from 0 to 2.5 ps, for the second isocyanide migratory insertion from adduct **5** to the bis-η^2-iminoacyl complex **6**. Time in ps and distances in Å.

Downloaded by CARLI CONSORTIUM on June 29, 2009
Published on August 28, 2002 on http://pubs.acs.org | doi: 10.1021/om020250j

Table 3. Optimized Geometrical Parameters (bond lengths in Å and angles in deg) of the MeNC Adduct 5 and Bis-η^2-iminoacyl Complex 6 Compared with the {p-Bu^t-calix[4](OMe)$_2$(O)$_2$Zr-[η^2-N(Bu^t)C(CH$_2$Ph)]$_2$} Complex[14]

parameters	5	6	exptl [ref 14]
R_{Zr-O_1}	2.089	2.082	2.054(4)
R_{Zr-O_2}	2.718	2.505	2.450(5)
R_{Zr-O_3}	2.073	2.082	2.054(4)
R_{Zr-O_4}	2.477	2.505	2.450(5)
R_{Zr-C_β}	2.430		
$R_{Zr-C'}$	2.288	2.296	2.259(6)
$R_{Z-N'}$	2.264	2.264	2.249(4)
$R_{C'-N'}$	1.281	1.281	1.271(8)
$R_{Zr-C''}$	2.329	2.296	2.259(6)
$R_{Zr-N''}$	-	2.264	2.249(4)
$R_{C''-N''}$	1.187	1.281	1.271(8)
$R_{C_\beta-C''N''}$	2.339	1.502	-
$\angle O_1ZrO_3$	96.2	97.5	91.9(1)
$\angle O_2ZrO_4$	144.4	145.5	143.8(1)
$\angle ZrC'N'$	72.6	72.3	73.2(3)
$\angle ZrC''N''$	169.4	72.3	73.2(3)

arrangement of the two iminoacyl groups shown by the X-ray structure. The optimized structure, reported in Figure 8, shows two symmetric iminoacyl units, with $Zr-C'$, $-C''$ and $Zr-N'$, $-N''$ bond distances of 2.296 and 2.264 Å, respectively, and short $N'-C'$, $C''-N''$ distances (1.281 Å) characteristic of carbon−nitrogen double bonds. In Table 3 the optimized geometrical parameters are compared to experimental data for {*p*-Bu^t-calix[4](OMe)$_2$(O)$_2$ Zr[η^2-N(Bu^t)C(CH$_2$Ph)]$_2$}, the closest compound for which X-ray data are available. The computed structure is in good agreement with X-ray data, even if the $\angle O_1ZrO_3$ angle is still larger than the experimental value due to the presence of bulky benzyl groups in the experimentally characterized compound. The bis-η^2-iminoacyl complex **6** was found 34.3 kcal mol^{-1} below adduct **5**, therefore 38.5 kcal mol^{-1} more stable than the free reagents; moreover, optimization of the transition state structure for insertion of the second isocyanide molecule, $\mathbf{TS}_{5\rightarrow6}$, led to a negligible barrier of 0.3 kcal mol^{-1}.

To provide an estimate of the free energy barrier for MeNC coordination leading to **5**, we evaluated the translational contribution to the activation entropy for this intermolecular process applying the Sackur−Tetrode equation.[32] We compute a $\Delta S_{298}^{\ddagger}$ value of −36.9 cal K^{-1} mol^{-1}; this value leads to an entropic contribution of 11.0 kcal mol^{-1} at 25 °C, resulting in a free energy barrier of 11.5 (11.0 + 0.5) kcal mol^{-1}, well higher than the value computed for the intramolecular methyl-to-isocyanide insertion of **3a** to **4** assuming a negligible entropic contribution, 6.4 kcal mol^{-1}, and consistent with the experimental evidence that only the imine product **4** is observed at room temperature. On the other hand, at −80 °C the entropic contribution to MeNC coordination is 6.7 kcal mol^{-1} ($\Delta S_{193}^{\ddagger} = -34.7$ cal K^{-1} mol^{-1}), so that the two barriers are comparable (6.7 + 0.5 kcal mol^{-1} = 7.2 vs 6.4 kcal mol^{-1}) and the higher thermodynamic stability of **6** with respect to **4** (38.5 vs 12.2 kcal mol^{-1}) favors the intermolecular process.

Conclusions

The stepwise migratory insertion of methyl isocyanide into the zirconium−carbon bonds in [calix[4](OMe)$_2$-(O)$_2$ZrMe$_2$] has been investigated by means of both static and dynamic density functional calculations. Dynamics simulations have shown that methyl isocyanide insertion takes place via the initial formation of an η^1-iminoacyl species that is suddenly converted into the more stable η^2-isomer.

The energy profiles for the two pathways branching from the initially formed methyl-η^2-iminoacyl, i.e., (i) the intramolecular methyl to iminoacyl migration, leading to an η^2-bound imine, and (ii) the uptake of a second

(32) Atkins, P. W.; De Paula, J. *Physical Chemistry*, 7th ed.; Oxford University Press: Oxford, UK, 2002.

isocyanide molecule followed by insertion into the residual $Zr-CH_3$ bond to give a bis-η^2-iminoacyl complex, have been characterized with the aim of explaining the temperature selectivity of the overall reaction. Formation of the bis-η^2-iminoacyl species was found exothermic by 38.5 kcal mol^{-1} with a free energy barrier of 11.5 kcal mol^{-1} at 25 °C, dominated by the entropic contribution. Such a value is 5.1 kcal mol^{-1} higher than that computed for the intramolecular imine formation, in agreement with the experimental evidence that only the imine product is observed at room temperature. On the other hand, at −80 °C the barrier to MeNC coordination is reduced to 7.2 kcal mol^{-1}, a value comparable to that computed for the intramolecular imine formation (6.4 kcal mol^{-1}), so that the higher thermodynamic stability of the bis-η^2-iminoacyl with respect to the η^2-imine (38.5 vs 12.2 kcal mol^{-1}) favors the intermolecular process.

The different reaction patterns following the migratory insertion of carbon monoxide and isocyanides into the zirconium−carbon bond of [*p*-Bu^t-calix[4](OMe)$_2$-(O)$_2$Zr(Me)$_2$] are therefore determined by the relatively high barrier and low exothermicity computed for the intramolecular formation of the η^2-imine, which opens the possibility of observing a second isocyanide insertion to give a bis-η^2-iminoacyl at low temperature. On the other hand, the low energy barrier (2.3 kcal mol^{-1}) and high exothermicity (41.1 mol^{-1}) computed for the intramolecular insertion of an alkyl group into the acyl moiety lead to formation of the η^2-bound ketone as the only product of CO migratory insertion.

Acknowledgment. We thank Dr. Paolo Giannozzi for generating the Zr pseudopotential. Thanks are also due to the CNR (Progetto Finalizzato "Materiali Speciali per Tecnologie Avanzate II") for financial support.

Supporting Information Available: Time evolution of the $\angle O_2-Zr-C_\alpha-C_\beta$ and $\angle C-Zr-O_2-C_\alpha$ dihedral angles and time evolution of the $Zr-C_\beta$ and N−C distances and of the $\angle NCZrC_\beta$ dihedral angle for the methyl to iminoacyl migration. This material is available free of charge via the Internet at http://pubs.acs.org.

OM020250J

Downloaded by CARLI CONSORTIUM on June 29, 2009
Published on August 28, 2002 on http://pubs.acs.org | doi: 10.1021/om020250j